Macromolecules

pubs.acs.org/Macromolecules Article

Complete pH-Dependent Shape Recovery in Cubical Hydrogel Capsules after Large Osmotic Deformations

Veronika Kozlovskaya, Bing Xue, Maksim Dolmat, and Eugenia Kharlampieva*

Cite This: *Macromolecules* 2021, 54, 9712–9723 Read Online

ACCESS | Metrics & More | Article Recommendations | Supporting Information

ABSTRACT: Polymeric colloids with reversible shape transformations have attracted increasing interest as stimuli-responsive biomimetic microsystems. We present cubical poly(methacrylic acid) (PMAA) hydrogel capsules that completely and reversibly collapse in response to osmotic pressure differences induced with poly(styrene sulfonate sodium salt) (PSS). The capsules with nanothin highly hydrated walls are synthesized through a multilayer assembly approach using 5 μm cubical sacrificial templates. The degree of capsule deformation in response to osmotically induced stresses and shape recovery upon stress removal were controlled by network crosslink density, PMAA ionization, and PSS concentration. The capsules deform alongside the cubical faces through inward face buckling under small osmotic pressures (6−20 kN m^{-2}), but they fully buckle inward in faces and edges, preserving uncollapsed vertices at higher osmotic pressures (>33 kN m^{-2}). Unlike immediate shape recovery after PSS removal at pH = 8, a prolonged relaxation for up to 3 days is observed at pH = 3. The observed deformation behavior suggests a uniform response to applied pressures due to initial rigidity points such as vertices and edges. Our study brings fundamental knowledge about the elastic deformations of nonspherical hydrogels, which can be essential in developing adaptable systems in controlled delivery, sensing, and microfluidics.

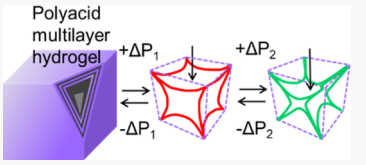

INTRODUCTION

The majority of biological micro- and nanoparticles, such as viruses, cells, and bacteria, have nonspherical shapes and adjustable stiffness that help regulate their transport across biobarriers and adhesion to target sites.[1−3] For example, acute promyelocytic leukemia cells become significantly softer to achieve migration capability.[4] Discoidal platelets can transform to spheroid shape upon various stimuli, which is a prerequisite for platelet activation.[5] The polygon-to-spindle shape deformation occurs in tumor cells to promote their invasive growth.[6]

Thus, the ability to create nano- and microsized particles of well-defined shapes provides a powerful means to optimize drug delivery carriers for specific therapeutic purposes. Using shape engineering technologies such as particle replication in nonwetting templates (PRINT),[7,8] stretching of films with embedded polystyrene spheres,[9] and template-induced printing,[10] polymeric microparticles with a broad range of well-defined geometries have been produced. Among these, polymer hydrogels allow for mimicking the shape of biological objects and their shape-dependent biological interactions.[11,12]

Low rigidity is among the advantages of polymeric hydrogels, allowing for control of their biomimicking properties.[13−15] For example, decreasing the elastic modulus of polyethylene glycol (PEG) nanogels from 3000 to 10 kPa increased their circulation *in vivo*.[16] The eightfold lowered elastic modulus of PRINT hydrogels resulted in a 30-fold increase in their circulation half-life.[17] The low elasticity can also regulate particle association with immune cells and improve the accumulation in targeted sites.[16,18,19] Thus, softer nanoliposomes with Young's modulus of 45 kPa were shown to be 2.6-fold more efficient in accumulating in 4T1 tumors compared to more rigid particles with Young's modulus of 19 MPa.[20] The soft particles with Young's modulus less than 1.6 MPa were found to accumulate more in tumor tissues, while most of their stiffer counterparts (Young's modulus > 13.8 MPa) stayed in the liver.[20] Recently, the more deformable yolk−shell mesoporous organosilicas with lower Young's modulus of 2.4 MPa were shown to facilitate their uptake by human breast cancer cells.[21]

Conversely, varying the hydrogel drug carrier's shape was shown to control the mechanical flexibility necessary for a hydrogel particle to successfully navigate through blood vasculature under pressure differentials observed in human capillaries. For instance, 8 μm-sized hydrogel disks, rings, crosses, and S-shapes obtained by polymerization of PEG diacrylate had different deformabilities as a function of their microstructure.[22] Discoid-shaped microgels with a very low elastic modulus (<17 kPa) were shown to pass through the channel pore of a twofold smaller diameter and recover their initial discoidal shape, while the more rigid discoids rapidly clogged the pores.[23] Similarly, PRINT hydrogel particles with a filamentous shape could pass through pores with much smaller diameters than the particle size.[24]

Received: March 23, 2021
Revised: August 25, 2021
Published: October 6, 2021

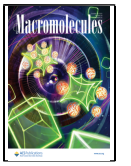

https://doi.org/10.1021/acs.macromol.1c00650
Macromolecules 2021, 54, 9712−9723

Polymeric capsules made via layer-by-layer (LbL) sequential assembly of polymers through electrostatic, hydrogen bonding, and covalent interactions have been established as a facile platform for biomedical and biotechnology applications.[25,26] This method allows for fabricating capsules of any size, geometry, composition, and thickness controlled at the nanoscale via alternating deposition of water-soluble polymers at solid/water interfaces to produce multilayer shells.[27] When these multilayer shells are crosslinked, nanostructured multilayer hydrogels can be obtained.[28] The covalent links stabilize the hydrogel capsule wall upon core dissolution, while functional groups which are not involved in binding provide stimuli-responsive behavior.[29] Since the hydrogel wall of a capsule is unconstrained after core dissolution, the thermodynamic force of mixing leads to hydrogel swelling due to the increased osmotic pressure, while the network's elastic retractive force opposes swelling.[30] The capsule wall stiffness, which resists the capsule's deformation, is directly proportional to the capsule wall thickness and inversely proportional to the particle size.[31] Despite the inherent softness and swelling ability of the hydrogel capsule wall, nonspherical multilayer hydrogel capsules that follow the template particles' shape after template dissolution have been demonstrated.[32] The hydrogel crosslink density and its pH sensitivity and the availability of cationic or anionic groups were shown to define the size and type of encapsulated molecules within the hydrogel capsule shell or its hollow cavity.[33−35]

Unlike continuous hydrogel particles, multilayer hydrogel capsules exhibit greater deformability than a filled hydrogel particle of the same shape. For instance, 7 μm discoidal capsules of poly(allylamine hydrochloride) (PAH) crosslinked with glutaraldehyde squeezed through a 5 μm glass capillary tip and recovered their original shape.[36] Notably, this discoidal capsule's elasticity modulus was in the order of hundreds of MPa, which was much larger than the passage threshold for filled discoidal PRINT hydrogels.[23] Therefore, the hollow capsule interior resembling a flexible cell membrane wrapping the cell interior could facilitate a better shape recovery via fluid-like deformation of the capsule membrane, unlike continuous hydrogels. Furthermore, nonspherical shapes have been demonstrated to have better shape recovery than spheres after pressure-induced shape loss. For example, 90% of discoidal $(PAH)_{10}$ capsules recovered their shape when passing through smaller pores, unlike spherical hydrogel capsules of the same composition and size, which showed only 63% shape recovery.[36] Besides, we have shown that 2 μm hollow cubical capsules with a low elasticity of 0.6 MPa could extravasate through much smaller 0.8 μm membrane pores under 18 psi pressure.[37]

Studies on the mechanical stability of nonspherical capsules have been limited to a few examples of relatively rigid ionic[38] and hydrogen-bonded LbL[37] structures compared to soft hydrogel capsules. For example, Caruso's group has shown that ionically paired poly(styrene sulfonate sodium salt) (PSS)/PAH microcapsules of dodecahedral shape (polyhedron with 12 rhombic faces) had enhanced stiffness compared to spherical capsules.[38] A computational study of spherical, cubical, and tetrahedral hydrogen-bonded tannic acid/poly(*N*-vinylpyrrolidone) (TA/PVPON) multilayer capsules suggested that sharp edges and vertices may introduce reinforcement against random buckling compared to spherical microcapsules.[39] Spherical and cylindrical poly(methacrylic acid) (PMAA) hydrogel capsules were shown to undergo deformations during cell internalization depending on the cell type.[40] Therefore, understanding how nonspherical hydrogel capsules deform under various pressures and what affects the recovery of their nonspherical shape is crucial for developing the next generation of elastic materials. Furthermore, controlling both the onset of buckling and the time required for shape recovery is essential for optimizing hydrogel capsule design.

Herein, we report on the development of cubical hydrogel microcapsules of 5 μm size and a capsule wall made of a 10-layer PMAA hydrogel obtained via the templated assembly of PVPON and amine-containing copolymers of PMAA and their deformation behavior in solution at pH = 3 and pH = 8. In bulk, the capsule deformation was studied in response to osmotic stress induced by PSS added to the solution to generate an osmotic pressure difference across the capsule thin shell. The (aminopropyl) methacrylamide copolymers of PMAA with the amine group molar ratios of 2.5 and 6.4% are synthesized using free radical copolymerization to control crosslink density of the PMAA hydrogel capsule shell and characterized by H1 NMR spectroscopy and gel permeation chromatography (GPC). The effect of crosslink density on capsule shape stability after core dissolution and upon capsule swelling at pH = 8 was explored using optical fluorescence microscopy. Finally, we studied the pH-dependent deformations of the $(PMAA)_{10}$ hydrogel cubical capsules and the effect of pH on the complete recovery of the cubical shape after large deformations. Our study is the first example of the nonspherical capsules with a nanothin shell (86 nm dry thickness) and sharp vertices and edges that can quickly and fully restore their complex shape after large deformations. Our findings can be crucial for understanding elastic deformations in polymer particles with complex shapes to develop advanced, adaptable networks.

EXPERIMENTAL SECTION

Materials. *N*-(*tert*-butoxycarbonyl-aminopropyl)methacrylamide (*t*BOC) was obtained from Polysciences, Inc. PVPON (average M_w 10000 g mol^{-1}), poly(ethylenimine) (PEI, average M_w 25000 g mol^{-1}), *tert*-butylmethacrylate (*t*BMA), 2,2′-azobis(2-methylpropionitrile) (AIBN), and PSS (M_w = 70000 g mol^{-1}) were purchased from Millipore-Sigma. Poly(glycidyl methacrylate) (PGMA, M_w ∼30000 g mol^{-1}) was synthesized by free radical polymerization as described earlier.[41] 1-Ethyl-3-(3-(dimethylamino)propyl)-carbodiimide hydrochloride (EDC) was obtained from Chem-Impex International. Monobasic sodium phosphate, hydrochloric acid, sodium hydroxide, ethylenediaminetetraacetic acid (EDTA), 1,4-dioxane, methanol, chloroform, dichloromethane (DCM), and trifluoroacetic acid (TFA) were from Fisher Scientific and used as received. Ultrapure deionized (DI) water with a resistivity of 18.2 MΩ cm was used in all experiments (Evoqua). Alexa Fluor 488 hydrazide was purchased from ThermoFisher.

Synthesis of Poly(methacrylic Acid-*co*-(aminopropyl)-methacrylamide) Copolymers, PMAA−NH_2−*m*. Statistical copolymers with amine-containing units, PMAA−NH_2−*m*, were synthesized using free radical polymerization as reported earlier.[42] The molar ratio of amine group-containing monomer units in the copolymer (*m*) was varied by the initial feeding ratio of *t*BOC to *t*BMA. Briefly, to prepare PMAA−NH_2−2.5, 0.175 g of *t*BOC was dissolved in 5 mL of dioxane and filtered with a 0.2 μm filter. Then, 2.056 g of distilled *t*BMA, *t*BOC solution, and AIBN recrystallized from methanol and 5 mL of dioxane were placed in a seal tube. The mixture was degassed by two freeze−pump−thaw cycles followed by backfill with nitrogen and heated to 65 °C. The reaction was quenched after 3 h by immersing the seal tube in a dry ice/acetone mixture. The copolymers were purified by a solvent/nonsolvent

https://doi.org/10.1021/acs.macromol.1c00650
Macromolecules 2021, 54, 9712−9723

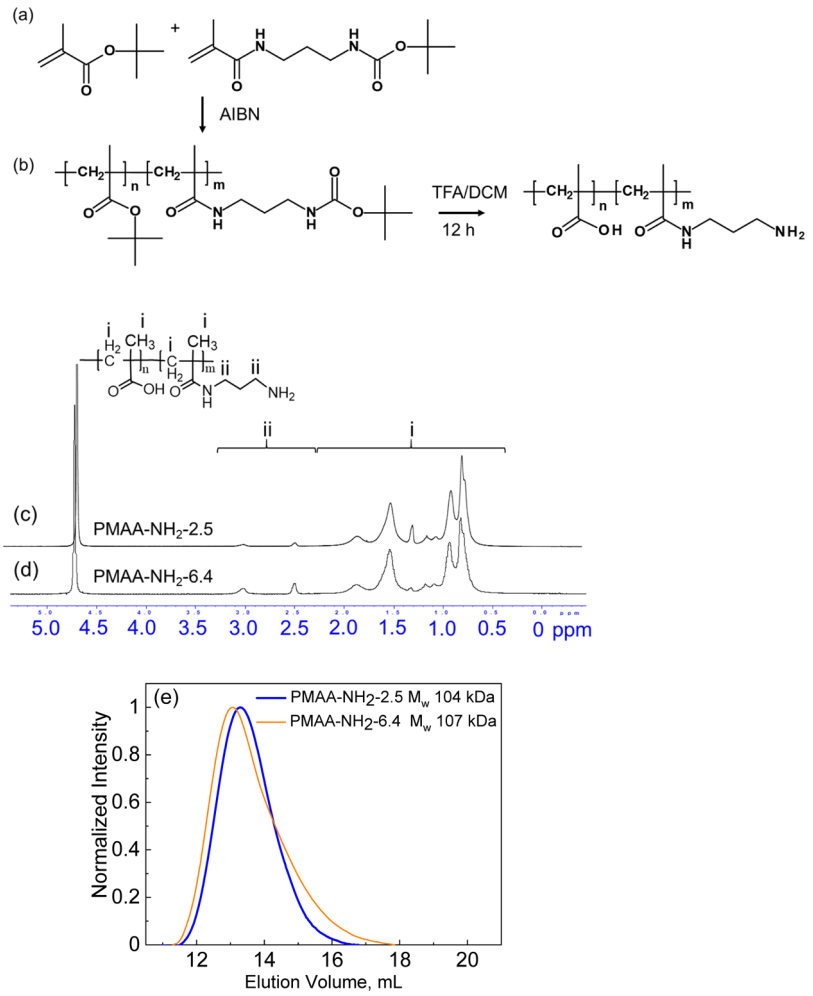

Figure 1. (a,b) Synthesis of the PMAA-*co*-((aminopropyl)methacrylamide) (PMAA−NH_2) copolymer. ^{1}H NMR spectra of (c) PMAA−NH_2−2.5 and (d) PMAA−NH_2−6.4 copolymers. (e) GPC traces of PMAA−NH_2−2.5 (solid thick) and PMAA−NH_2−6.4 (solid thin) copolymers.

method. The mixture was added dropwise into a 10-fold excess of water/methanol (1:4, v/v). The precipitated copolymer was redissolved in DCM, precipitated in water/methanol (1:4, v/v) twice, and dried in a vacuum. The copolymers were deprotected in 10% (v/v) TFA in DCM overnight. The deprotected PMAA−NH_2−2.5 was dialyzed in DI water (MWCO 6−8 kDa, Fisher Scientific) for three days. For the synthesis of the PMAA−NH_2−6.4 copolymer, 0.512 g of *t*BOC was used for the polymerization at 70 °C for 2 h. The composition of PMAA−NH_2−*m* copolymers was determined using proton nuclear magnetic resonance spectroscopy (^{1}H NMR). ^{1}H NMR spectra of the copolymers (10 mg mL^{-1} in D_2O containing 0.05 mL NaOD) were collected on a Bruker 700 MHz NMR spectrometer. The weight-average molecular weights of PMAA−NH_2−*m* copolymers before deprotection were determined by GPC in THF (GPC, Waters) using linear polystyrene standards (Waters).

Surface-Anchored PMAA Multilayer Hydrogels. Hydrogen-bonded (PVPON/PMAA−NH_2)$_n$ multilayers, where *n* denotes the number of polymer bilayers, were assembled on silicon wafers (University Wafer) using dipping LbL. First, a PGMA/PMAA precursor was covalently attached to the wafer surface to anchor the multilayer hydrogel to the surface.[43] For that, PGMA chloroform solution (0.09 mg mL^{-1}) spin-coated onto a wafer was heated for an hour at 110 °C in an oven. Unattached PGMA was rinsed off using chloroform three times. Subsequently, PMAA (1 mg mL^{-1} in methanol) was spin-coated onto the PGMA layer and covalently linked to glycidyl groups by heating the wafer for 40 min at 88 °C in an oven. Unattached PMAA was rinsed off with DI water. The (PVPON/PMAA−NH_2−*m*)$_n$ multilayer was assembled from 0.5 mg mL^{-1} polymer solutions at pH = 2 (0.01 M HEPES, 0.1 M NaCl) with a 10 min deposition time. The multilayer film was crosslinked by exposure to EDC solution (5 mg mL^{-1}) at pH = 5 for 1 h, followed with a 0.01 M HEPES buffer at pH = 5.5 for 2 h and at pH = 5.8 overnight. After that, the film was transferred to pH = 8 (0.01 M HEPES buffer) for 24 h to release PVPON from the PMAA multilayer hydrogel.

Ellipsometry. The thickness of multilayer hydrogels was measured using an M2000U spectroscopic ellipsometer (J. A. Woollam). For dry thickness, films were dried under a gentle nitrogen flow and measured at 65, 70, and 75° angles of incidence in the wavelength range from 400 to 1000 nm. The ellipsometric angles Ψ and Δ were fitted using a multilayer model composed of Si, SiO_2, and the Cauchy film to obtain the film thickness. The SiO_2 thickness for each wafer was measured using known optical constants. The thickness of the hydrogel film was extracted fitting with the Cauchy approximation. Film swelling in solutions of varied pH values was measured using a 5 mL liquid flow-through cell (J. A. Woollam). The cell was filled with 0.01 M phosphate buffer solutions at various pH values, and the data were collected after 15 min equilibration. These data were fitted with the Cauchy approximation with the permitted fitting of A_n, B_n, and C_n. The mean squared error for data fitting was less than 20.

Synthesis of Cubical (PMAA) Multilayer Hydrogel Capsules. The hollow capsules were prepared by coating cubical Mn_2O_3 microparticles[44] with PEI (PMAA−NH_2−m/PVPON)$_{10}$ multilayers followed by crosslinking of PMAA. The PEI layer was adsorbed on the particle surface from 0.5 mg mL^{-1} aqueous solution (pH = 6). The PMAA−NH_2 and PVPON adsorbed from 0.5 mg mL^{-1} polymer

https://doi.org/10.1021/acs.macromol.1c00650
Macromolecules 2021, 54, 9712−9723

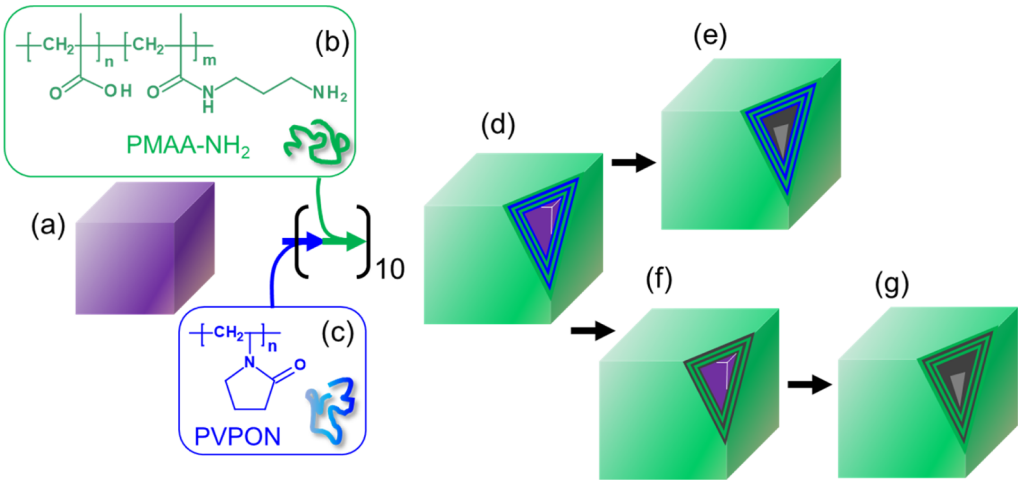

Figure 2. Schematics for the multilayer assembly of cubical (PMAA) multilayer hydrogel capsules. Manganese oxide cubical cores (a) were alternatingly exposed to polymer solutions of PMAA−NH_2 (b) and PVPON (c) in aqueous solutions at pH = 2 with two buffer rinses between the layers. After assembly of 10 bilayers of (PMAA−NH_2/PVPON) (d), hydrogen-bonded cubical shells of (PMAA−NH_2/PVPON) were obtained when the manganese oxide cores were dissolved (e). Conversely, when PMAA−NH_2 layers were crosslinked through carbodiimide-assisted covalent bonding of −COOH and $-NH_2$ groups and PVPON layers were released at pH = 8 (f), hollow cubical capsules with the shell composed of the $(PMAA)_{10}$ multilayer hydrogel were obtained after core dissolution in hydrochloric acid followed by dialysis and EDTA treatment (g).

solutions (0.01 M HEPES, 0.1 M NaCl; pH = 2) under shaking, starting from PMAA−NH_2. After each deposition step (10 min), the particles were centrifuged at 5000 rpm for 2 min to remove the excess polymer, followed by particle resuspension in 0.01 M buffer solution (0.01 M HEPES, 0.1 M NaCl) at pH = 2. The rinsing was repeated twice. The $(PMAA-NH_2/PVPON)_{10}$ multilayers were crosslinked as described for the films. For that, $(PMAA-NH_2/PVPON)_{10}$ core−shell particles were first treated with EDC at pH = 5, followed by pH = 5.5 and 5.8, as described for planar films, and pH = 8 (0.01 M HEPES buffer). Inorganic cores were dissolved in 6 M HCl to yield hollow $(PMAA)_n$ hydrogel capsules. The 0.1 M EDTA (pH = 7.2) solution was added to the hydrogel capsules twice for 3 h to completely chelate manganese ions,[45] followed by dialysis in DI water for 3 days (MWCO 20 kDa, SpectrumLabs).

Optical Fluorescence Microscopy. pH-triggered capsule size/shape changes were examined using a Nikon optical fluorescence microscope equipped with a 60× oil immersion objective. Capsules (25 μL; 10^8 capsules mL^{-1}) were added to a Lab-Tek chambered coverglass (Electron Microscopy Sciences) filled with a buffer solution at the desired pH. A fluorescent dye, Alexa Fluor 488 hydrazide (Ex/Em = 493/517 nm), was added (10 μL) to the chamber to visualize the capsules, and optical fluorescence images were collected. The Alexa Fluor 488 hydrazide dye (Figure S1) was trapped inside the capsule shell network due to hydrophobic or hydrogen bonding interactions due to the presence of hydrazide and amine moieties of the dye, which resulted in fluorescence from the capsule walls at pH = 3 and pH = 8. For PSS-induced capsule buckling, the capsules were mixed with PSS solutions (450 μL) of varying concentrations (wt %) at pH = 3 or pH = 8. The highest concentration of sodium ions from PSS was very low (0.04 M), resulting in a low ionic strength. Therefore, the effect of the ionic strength from sodium ions in PSS on the PMAA hydrogel was not considered to be significant in this work. The number of deformed and intact capsules was determined by analysis of the images using ImageJ software (Figures S2 and S3). The marker lines were drawn through a capsule image at a region of interest, and the intensity−distance profiles were generated using ImageJ software. The intensity−distance profiles were plotted using OriginPro software, and the markers at the maximum intensities were used to determine the distance (μm) between the markers and, consequently, the faces of the cubical capsules before and after exposure to PSS. In total, 100 capsules in separate areas of three view fields were analyzed for each PSS concentration. Shape recovery of deformed capsules was examined after the PSS solution was replaced with a 0.01 M phosphate buffer solution at pH = 3 or pH = 8 by five solution exchanges in the chambered coverglass. The optical fluorescence images of the capsules were collected after the solution replacement and analyzed as described above.

ζ-Potential Measurements. For surface charge analysis of the hydrogel capsules, a ζ-potential of capsule solution was measured in 0.01 M phosphate buffer at pH = 3 using a Nano-ZS Zetasizer (Malvern) equipped with a He−Ne laser (663 nm). The capsule solution (10^6 capsules per milliliter) was transferred into a disposable ζ-potential cuvette and incubated at pH = 3 and 25 °C for 2 min. The average value of the ζ potential was obtained from three measurements with 12 runs each.

Atomic Force Microscopy. The capsule single-shell thickness was obtained from the atomic force microscopy (AFM) topography images of capsules using an NT-MDT NTEGRA atomic force microscope. The AFM silicon probes NSG30 (NT-MDT, resonance frequency 300 kHz, force constant 22−100 N m^{-1}, tip radii 5 nm) were used at a scan rate of 0.6−1 Hz to collect capsule images in the dry state. For imaging, a drop of a capsule solution was dried on a freshly cleaned Si wafer (0.5 cm^2) and scanned in the air. The single-wall thickness of capsules was obtained as half of the height of the collapsed flat regions of dried capsules generated from AFM height histograms.

RESULTS AND DISCUSSION

Synthesis of Cubical Multilayer Hydrogel Capsules. First, two poly(methacrylic acid-*co*-(aminopropyl) methacrylamide) copolymers (PMAA−NH_2) with 2 M ratios of amine-containing units were synthesized via free radical copolymerization of *tert*-butyl methacrylate and *t*BOC using AIBN as an initiator (Figure 1a). The *tert*-butoxycarbonyl protective groups in the copolymers were then removed by overnight treatment with TFA in DCM (10%, v/v) (Figure 1b), as we described previously.[42] The amine groups were introduced to precisely control the crosslink densities in the PMAA multilayer hydrogels, as we demonstrated earlier for other multilayer hydrogels,[41,46] and pH-induced swelling of the PMAA nanostructured hydrogel. The molar ratios of amine-containing units within the PMAA−NH_2 copolymers were quantified by H^1 NMR (Figure 1c,d) and were found to be 2.5 and 6.4%. GPC analysis of the copolymers before the amine group deprotection using polystyrene linear standards

https://doi.org/10.1021/acs.macromol.1c00650
Macromolecules 2021, 54, 9712−9723

demonstrated a unimodal weight distribution with weight-average molecular weights of 104 and 107 kDa for PMAA–NH_2–2.5 and PMAA–NH_2–6.4, respectively (Figure 1e). Next, cubical multilayer hydrogel capsules were fabricated using a multilayer deposition of polymers on sacrificial templates, as we reported earlier.[42] For that, cubical manganese oxide particles of 5 μm size primed with a PEI monolayer[44] were coated with a 10-bilayer hydrogen-bonded film of (PMAA–NH_2/PVPON) deposited stepwise at pH = 2 from aqueous polymer solutions (Figure 2a–d). When the inorganic template particles were dissolved in concentrated HCl (6 M), the cubical capsules made of the hydrogen-bonded (PMAA–NH_2/PVPON) multilayer were obtained (Figure 2e). Conversely, the core–shell $(PMAA)_{10}$ particles with the PMAA multilayer hydrogel shell were obtained when the $(PMAA–NH_2/PVPON)_{10}$ core shells were exposed to carbodiimide solution to crosslink PMAA–NH_2 layers within the polymer shell, followed by the release of uncrosslinked PVPON at pH = 8 (Figure 2f). Finally, the dissolution of the inorganic manganese oxide cubical templates resulted in hollow $(PMAA)_{10}$ capsules (Figure 2g). The capsules were dialyzed at pH = 3 and soaked in an aqueous solution of the fluorescent Alexa 488 dye for capsule visualization using optical fluorescent microscopy.

Using the abovementioned procedure, the 10-layer multilayer hydrogel capsules obtained from PMAA–NH_2–6.4 and PMAA–NH_2–2.5 copolymers, denoted as $(PMAA^*)_{10}$ and $(PMAA^{**})_{10}$, respectively, replicated the cubical shape of the template upon the core dissolution and exhibited well-defined vertices, faces, and edges after dialysis at pH = 3 (Figure 3a,b).

We found that after chelating manganese ions with EDTA from the hydrogel shell, the $(PMAA^{**})_{10}$ capsules lost their defined cube geometry, unlike the $(PMAA^*)_{10}$ capsules that retained the cubical shape of the template (Figure 3c,d). This difference agrees with the lower ratio of amine units in the PMAA–NH_2–2.5 chain and, therefore, the lower crosslink density of the PMAA** hydrogel shell compared to that of the PMAA* hydrogel shell.

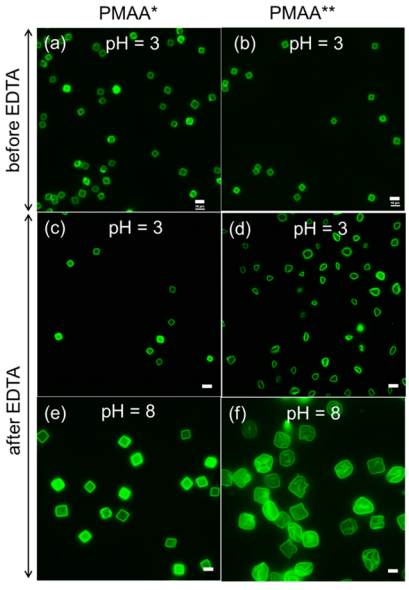

Figure 3. Optical fluorescence microscopy images of 10-layer PMAA* (a,c,e) and PMAA** (b,d,f) multilayer hydrogel capsules assembled from PMAA–NH_2–6.4 and PMAA–NH_2–2.5 copolymers, respectively. The capsules are shown at pH = 3 (a–d) and pH = 8 (e,f); before (a,b) and after (c–f) EDTA treatment. The scale bar is 10 μm in all images.

Both EDTA-treated PMAA* and PMAA** cubical hydrogel capsules demonstrated a pronounced pH-dependent swelling when they were brought to pH = 8, as evidenced by the optical fluorescence images of the capsules in solution (Figure 3e,f). However, the more rigid $(PMAA^*)_{10}$ hollow cubes maintained a defined cubical shape even in their swollen state with the size measured side to side increasing from 4.9 ± 0.6 μm at pH = 3 to 9.0 ± 0.8 μm at pH = 8, while much more swollen softer $(PMAA^{**})_{10}$ capsules almost lost their cubical shape upon swelling with the size increase above 14 μm. In addition, the swollen $(PMAA^{**})_{10}$ cubical shells exhibited various degrees of capsule face and edge buckling (Figure 3f). The latter result agrees with our earlier observation of thinner PMAA hydrogel cubical capsules crosslinked with ethylenediamine that demonstrated bulging of the faces after EDTA treatment at high pH.[42,47] Similarly, the increased rigidity of spherical PMAA hydrogel capsules with the increased molar ratio of crosslinkable thiols from 5 to 20% was also reported by the Caruso group.[48,49]

Swelling behavior of 10-layer PMAA* and PMAA** planar multilayer hydrogels anchored to the surface of a Si wafer that mimicked the capsule shell's swelling is shown in Figure 4. The

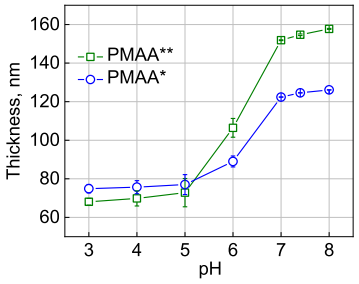

Figure 4. pH-dependent thickness changes of PMAA multilayer hydrogel films covalently anchored to Si wafer surfaces.

hydrogel films' pH-dependent thickness measurements using *in situ* ellipsometry revealed a larger swelling of the softer PMAA** hydrogel compared to that of the more rigid PMAA* hydrogel. For example, the thickness of the $(PMAA^*)_{10}$ multilayer hydrogel showed a 1.7-fold increase from 75 ± 2 nm at pH = 3 to 126.1 ± 0.1 nm at pH = 8 (Figure 4, circles), while a 2.3-fold thickness increase was observed for the $(PMAA^{**})_{10}$ hydrogel from 68 ± 2 nm at pH = 3 to 157.7 ± 0.3 nm at pH = 8 (Figure 4, squares). Note a slightly larger shrinkage of the PMAA** hydrogel at the low pH due to more coiling of the more flexible PMAA chain between two crosslinks (41 monomer units for PMAA** *vs* 16 units for PMAA*) due to the lower crosslink density. A similar shrinkage behavior was reported for spherical PMAA multilayer hydrogel capsules crosslinked with ethylenediamine.[34] Also, the ellipsometry data in Figure 4 demonstrate that in contrast to the PMAA multilayer hydrogels crosslinked with ethylenediamine or cystamine that swelled both in the low (pH < 5)- and high-pH (pH > 6) regions,[44,50] the hydrogel obtained from the PMAA–NH_2 copolymer had no thickness increase at pH < 5. The result indicates that all amine groups in the copolymers' methylacrylamide units participated in crosslinking with –COOH groups of PMAA layers.

https://doi.org/10.1021/acs.macromol.1c00650
Macromolecules 2021, 54, 9712–9723

Large Reversible Deformations of Cubical Hydrogel Capsules at Basic pH. As shown earlier,[31,51,52] the spherical capsule shell loses its shape and transforms to a concave inward-buckled shape when the external pressure work equals the deformation energy. We studied large deformations of the hollow $(PMAA^*)_{10}$ hydrogel cubes using an osmotic buckling approach that was applied for mechanical analysis of both ionically paired and hydrogen-bonded capsules.[31,53,54] The PMAA* cubical hydrogel capsules were selected because they, unlike $(PMAA^{**})_{10}$, could maintain their cubical shape at low and high pH values (Figure 3). The capsules stained with Alexa Fluor 488 fluorescent dye were exposed to varying PSS concentrations at pH = 8, and their shape transformations were observed using optical fluorescence microscopy. The neutral molecules such as PEG and dextran could also be used to explore capsule shell deformation, given that they are excluded from the capsule interior under experimental conditions. Indeed, the osmotically induced deformation of cells and nonionic gels has been explored in the presence of dextran sulfate, where cells or gels shrank via an osmotic shock.[55] The PEG was not selected for our experiments due to its hydrogen bonding with PMAA at low pH, and we used PSS instead, as was reported in previous studies on polyelectrolyte capsule deformation.[31,51]

Figure 5 shows that in the presence of 0.1% PSS sodium salt, the cubical capsules exhibited a slight inward face bulging (Figure 5a), which further increased when a higher concentration of PSS (0.3%) was used (Figure 5b). Even more severe deformations of the cubical hydrogel capsules occurred at higher PSS concentrations of 0.5 and 1%, resulting in a complete inward collapse of the cube faces and the shape transformation from the cubical to the star-like shape (Figure 5c,d). This deformation behavior is due to the exclusion of PSS macromolecules of 70 kDa by the $(PMAA^*)_{10}$ hydrogel shell, which is permeable to small water molecules. This semipermeability leads to the osmotic pressure difference between the capsule's interior and the bulk, and the solution is squeezed out from the capsule interior when the elastic force of the hydrogel shell cannot compensate for the induced pressure difference (Figure 5e–g). The unlabeled capsules demonstrated similar buckling behavior as those labeled with the fluorophore (Figure S4). Remarkably, even the fully collapsed hydrogel capsules could completely restore their initial cubical shape within a few minutes after removing PSS, followed by rinsing with a 0.01 M phosphate buffer at pH = 8 (h-k).

The observed deformation behavior is similar to that reported for cubical hydrogen-bonded 15.5-bilayer (TA/PVPON) capsules, where the capsules buckled with the cubical faces collapsed inside the capsule volume upon drying with a few cube edges bent as well.[56] Our results also agree with the buckling behavior predicted by molecular dynamics simulations for cubical polymeric shells in solution upon a decrease in internal pressure and due to inhomogeneous strain–stress distributions alongside the sharp corners and edges of the cube.[39]

The analysis of capsule dimensions upon these small deformations revealed that the diagonal size of the capsules, D (Figure 6a), remained unchanged for small deformations induced by 0.1 and 0.3% PSS and was measured to be 12.3 ± 1.1 and 11.4 ± 0.9 μm, respectively, which is the same as the diagonal size of 12 ± 1 μm for the initial capsules before PSS exposure. The initial side-to-side distance, s = 9 ± 1 μm (Figure 6a), of untreated capsules decreased to the deformed

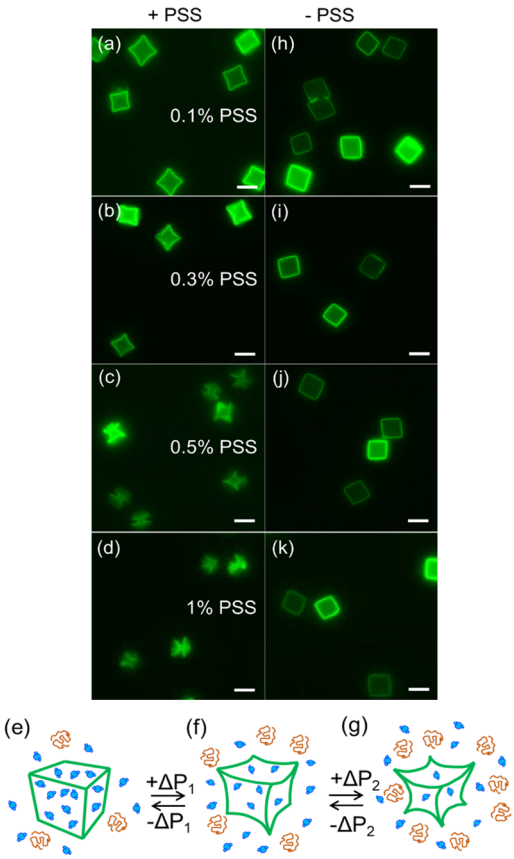

Figure 5. Optical fluorescence images of the cubical $(PMAA^*)_{10}$ hydrogel capsules in buffer solution at pH = 8 in the presence of PSS (a–d) of 0.1 wt % (a), 0.3 wt % (b), 0.5 wt % (c), and 1 wt % (d) and after PSS was rinsed off with buffer at pH = 8 (h–k). The scale bar is 10 μm in all images. The schematics (e–g) shows a cubical PMAA capsule (e) that reversibly deforms in response to osmotic pressure differences ΔP_1 (f) and ΔP_2 (g) at pH = 8, where $\Delta P_2 > \Delta P_1$.

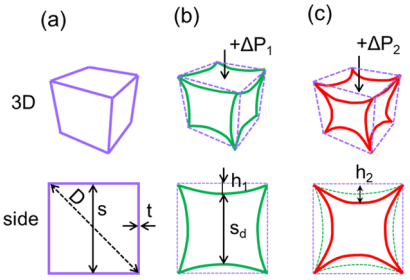

Figure 6. Three-dimensional and side views of a cubical $(PMAA^*)_{10}$ multilayer hydrogel capsule in an aqueous solution before (a) and after (b,c) deformation due to osmotic pressure differences (ΔP_1 and ΔP_2) induced with varied concentrations of PSS sodium salt. The cubical $(PMAA^*)_{10}$ hydrogel capsule before deformation [(a), side view] has the dimensions as s (a side-to-side capsule size) and D (a diagonal capsule size), with the shell thickness of t, and after deformation [(b), side view] as s_d (a side-to-side capsule size in the middle of the edge) and h (a maximum deflection of the cubical face, which is calculated as $h = (s - s_d)/2$, where D, s, and s_d are measured from optical fluorescence images, and dry shell thickness, t, is measured by AFM.

size, s_d, of 7.8 ± 0.1 and 6.5 ± 0.1 μm in the case of osmotic pressure differences ΔP_1 (Figure 6b) and ΔP_2 (Figure 6c) induced by 0.1 and 0.3% PSS, respectively. From the differences between the initial and deformed side-to-side

https://doi.org/10.1021/acs.macromol.1c00650
Macromolecules 2021, 54, 9712–9723

capsule sizes, the deflection (h_1 and h_2 in Figure 6b,c, respectively) due to the inward bulging of the square faces of the cubical hydrogel capsules was calculated as $h = (s - s_d)/2$ to be 0.6 and 1.25 μm for ΔP_1 and ΔP_2, respectively. Much larger capsule deformations induced with the PSS concentration of 0.5% or higher led to the loss of the diagonal dimension and almost total shrinkage of the capsule side-to-side distance (Figure 5c,d). However, it is worth noting that the capsule vertices behaved as the ultimate rigidity points that never collapsed, resulting in shrunken star-like hydrogel capsules.

Since the cubical capsules' diagonal size remained unchanged at PSS concentrations lower than 5%, the capsule's vertices and edges can be considered a rigid frame, and the capsule face can be viewed as a square flat film suspended over the square frame (Figure 6). Therefore, we evaluated the hydrogel shell elasticity by applying the thin-film bulging approach[57] to analyze a capsule face's inward deflection as a function of applied pressure. It was shown[57,58] that the pressure (P)−deflection (h) relation for a square membrane with deflections $h \gg t$, where t is the film thickness, can be expressed as (eq 1)

$$P = 3.393\frac{\sigma_0 \mathrm{th}}{s^2} + (1.996 - 0.613\nu)\frac{Et}{(1-\nu)}\frac{h^3}{s^4} \quad (1)$$

where σ_0 is the residual stress, s is the length of the membrane, E is Young's modulus, and ν is the Poisson ratio. From this, by plotting P/h as a function of h^2 as a straight line, one can determine $E/(1-\nu)$ from the best-fitted slope.[57]

The osmotic pressure from PSS solutions with varying concentrations was calibrated using a vapor pressure osmometer as described earlier.[53] The dry thickness of the $(PMAA^*)_{10}$ hydrogel capsule wall was obtained from AFM height analysis of flat regions of a dry capsule,[53,59] 86 nm for a single-wall thickness of a hydrogel capsule. The hydrated capsule wall thickness at pH = 8 was calculated to be 378 nm assuming the 4.4-fold swelling of the $(PMAA^*)_{10}$ hydrogel at pH = 8. This 4.4-fold swelling of the hydrogel was obtained from *in situ* ellipsometry thickness measurements of the planar hydrogel film from its dry state (28.6 nm) to its swollen state at pH = 8 (126.1 nm) (Figure 4, circles). From the $P/h = f(h^2)$ slope and $\nu = 0.3$ for polymer gels in a good solvent,[60] the elasticity modulus of $(PMAA^*)_{10}$ hydrogel capsules was estimated to be ~56 MPa. This result is in good agreement with the values of Young's modulus for elastomeric networks.[61] For example, Young's modulus of spherical hydrogen-bonded multilayer capsules assembled and measured at pH = 2 by AFM nanoindentation was found to be 610 ± 70 MPa,[62] while that for softer hydrogen-bonded capsules obtained from methanol and measured at pH = 3 by the osmotic pressure difference method was found to be 97 ± 8 MPa.[53] Conversely, lower Young's modulus of 20 kPa at pH > 6 was found for collapsed spherical capsules of crosslinked PMAA−NH_2 using AFM nanoindentation that can be attributed to the very low crosslink density of 100 monomer units between the crosslinks for that hydrogel shell.[63] Indeed, as demonstrated by Best *et al.*, the stiffness of PMAA multilayer hydrogel capsules obtained from thiolated PMAA was shown to increase at a greater rate with crosslinking in contrast to planar films of the same thickness due to a combination of increased material stiffness and enhanced shell structure that resists expansion.[48]

To further investigate the reversibility of large capsule deformations, the $(PMAA^*)_{10}$ cubical capsules were exposed to a large PSS concentration (5 wt %), and the capsule shape response was observed with optical fluorescence microscopy for two cycles. In the presence of 5 wt % PSS, all capsules completely buckled to a star-like shape (Figure 7a). However,

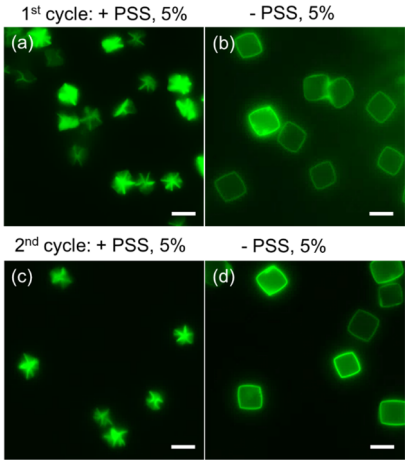

Figure 7. Optical fluorescence images of $(PMAA^*)_{10}$ hydrogel capsules in the presence of 5 wt % of PSS (a) and after PSS removal during the first cycle at pH = 8 (b). The capsules (b) after second addition of 5 wt % of PSS (c) at pH = 8 and after PSS was rinsed off with buffer at pH = 8 for the second time (d). The scale bar is 10 μm in all images.

after PSS removal, the capsules fully restored their initial cubical shape with well-defined edges and vertices within 30 min (Figure 7b). The same complete restoration of the capsule shape was observed when the process was repeated (Figure 7c,d), confirming a reversible shape change of the cubical $(PMAA^*)_{10}$ hydrogel capsules. Importantly, the surface charge measurements performed on the pristine capsules at pH = 7 and after their exposure to 3 wt % solution of PSS in DI water for 30 min followed by six rinses with 0.01 M phosphate buffer at pH = 7 did not show any PSS adsorption on the capsule wall at pH = 7. The ζ potential values of the capsules before and after the PSS exposure were −39 ± 2 and −37 ± 1 mV, respectively (Figure S5a). These results are, in fact, expected due to the mutual repulsion between PSS and the PMAA network, which are both negatively charged at pH = 7.

These results show the first example of complete shape reversibility for nonspherical capsules without smooth surfaces and with 8 vertices and 12 edges after large deformations. The shape loss due to osmotic buckling was observed previously only in spherical capsules and was generally irreversible. Thus, the ionically paired PSS/PAH spherical capsules could not completely regain their shape when the deformation extent was larger than 34% after being squeezed through a microchannel.[64] Earlier, Gao and co-workers demonstrated that discoidal capsules of the PAH multilayer hydrogel obtained *via* glutaraldehyde crosslinking could reversibly deform while being squeezed through a channel narrower than the capsule size capillary.[65] These discoidal hydrogel capsules had the elasticity modulus in the hundreds of MPa range. In our earlier work on the pH-triggered shape change of cubical hydrogel capsules, pH-induced swelling of the cubical $(PMAA)_{13}$ hydrogel capsule shell led to partial shape reversibility due to the presence of both covalent and ionic links in the network.[47]

https://doi.org/10.1021/acs.macromol.1c00650
Macromolecules 2021, 54, 9712−9723

Conversely, the pH-triggered swelling could induce a complete shape recovery for discoidal-to-ellipsoidal shape transformations of $(PMAA)_{15}$ hydrogel capsules with only covalent links in the hydrogel network.[46] The difference in the two network types was that the former contained covalent crosslinks and dynamic ion pairing, while the latter contained only covalent linkages.

Also, unlike the hydrogen-bonded spherical $(PVPON/PMAA)_{10}$ multilayer capsules reported earlier[53] with shape recovery within 12 h after stress release, the shape recovery of the $(PMAA^*)_{10}$ hydrogel cubical capsules in this work took place almost immediately after stress release. The complete and fast shape recovery after high deformations was also observed for bulk covalently linked polymeric gels.[66−68] Furthermore, the presence of rigid structural elements such as vertices and edges was suggested to contribute to the larger stability of nonspherical dodecahedral multilayer capsules of (PSS/PAH)[38] toward small compressive stresses, unlike spherical capsules of the same material and thickness. These reinforcement elements in the (PMAA*) cubical hydrogel capsules may be an additional factor responsible for the full shape recovery of the (PMAA*) cubical capsule.

Deformations and Recovery of Cubical $(PMAA^*)_{10}$ Hydrogel Capsules at Acidic pH. We also studied osmotically induced deformations of $(PMAA^*)_{10}$ cubical capsules at low pH. Since the hydrogel deswells at pH = 3 (Figure 4) due to the protonation of carboxylic groups and hydrophobic coiling of PMAA segments, the hydrogel capsules decreased in size without a change in shape (Figure 3c). The surface charge of the hydrogel capsules at pH = 3 (0.01 M phosphate buffer) was neutral with the ζ-potential of -1.5 ± 0.2 mV as measured using a Nano ZS Zetasizer (Malvern) (Figure S5b). This result indicates that at low pH, all amine groups were completely consumed by the crosslinking with the carboxylic groups of the network. This agrees with the hydrogel thickness measurements using *in situ* ellipsometry (Figure 4) that revealed no hydrogel swelling at pH < 5 (pK_a of PMAA 5.2−6),[69] and therefore, no free amine groups remained after crosslinking. Hence, no ionic pairing was expected between anionic PSS and the neutral capsule shell network.

Because of the size decrease due to the shell deswelling, the capsules became stiffer and did not show the inward buckling of faces at the PSS concentrations lower than 3 wt % with the size $s = 4.9 \pm 0.6$ μm in the presence of 1 wt % PSS at pH = 3 (Figure 8a, inset). The low inward deformations of cubical faces were observed starting at 3 wt % PSS (Figure 8a), with the capsule side-to-side distance decreasing to s_d 3.3 ± 0.4 μm but maintaining the diagonal distance $D = 5.9 \pm 0.2$ μm, similar to that for the intact capsules ($D = 6.0 \pm 0.5$ μm). At higher, 5 wt % PSS concentration, the capsules completely buckled inward with the cubical shape's loss (Figure 8f).

In contrast to almost immediate regaining of cubical shape at pH = 8 after stress release, the capsules at pH = 3 demonstrated persistent deformations even 30 min after the PSS removal for both PSS concentrations (Figure 8b,g). After 3%wt PSS was rinsed off, the 24 h incubation of the capsules in 0.01 M phosphate buffer at pH = 3 resulted in the slight capsule relaxation to a less-concaved shape (Figure 8c). In contrast, the ones treated with 5 wt % PSS still demonstrated a full inward buckling of the faces 24 h after the stress release (Figure 8h), slowly releasing the deformations after 3 days of incubation in the 0.01 M phosphate buffer at pH = 3 (Figure 8h, inset). The surface charge measurements of the capsules performed before (1.5 ± 0.2 mV) and after (-39.7 ± 1.9 mV) their exposure to 3 wt % PSS solution for 30 min at pH = 3 revealed that PSS can be adsorbed at the surface of the deswollen capsules at pH = 3, which is observed as the increased negative surface charge of the shell (Figure S5b). Although the capsule rinsing with pH = 3 buffer failed to remove the adsorbed PSS, the following rinsing with pH = 7 (-33 ± 2 mV) followed by rinsing with pH = 3 (-1.6 ± 0.1 mV) was successful in the PSS removal from the capsule wall (Figure S5b). After that, the capsule ζ-potential reverted to the initial ζ-potential value before the PSS exposure. These data suggest that the slow relaxation of the capsules after PSS rinsing can be attributed to PSS adsorption on the capsule wall at pH = 3. At this pH, two types of links are present in the shell network: permanent amide linkages and dynamic hydrogen bonds. Intermolecular hydrogen bonding between two carboxylic groups of adjacent polyacid molecules[70] and between amide bonds and protonated carboxylic groups[71] can contribute to the dynamic hydrogen bonds within the network at low pH, rendering it hydrophobic, which would facilitate adsorption of PSS.

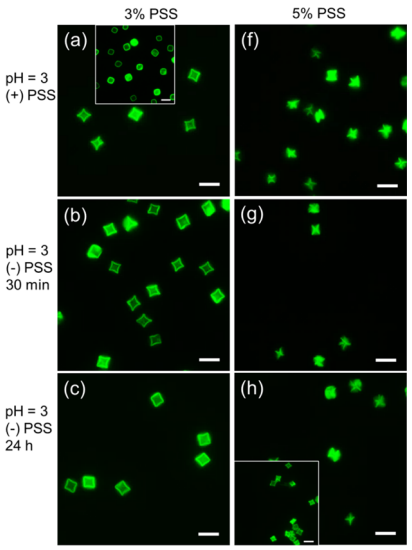

Figure 8. Optical fluorescence images of the $(PMAA^*)_{10}$ hydrogel capsules deformed in the presence of 1 wt % [(a), inset], 3 wt % (a), and 5 wt % (f) PSS at pH = 3. The images were taken within 30 min after the removal of 3 wt % PSS (b) and 5 wt % PSS (g) and 24 h after the removal of 3 wt % PSS (c) and 5 wt % PSS (h). The inset (h) shows the capsules (h) after 3 days at pH = 3. The scale bar is 10 μm in all images.

Indeed, when the cubical capsules deformed by their exposure to either 3 or 5 wt % PSS (Figure 8a,f, respectively) were exposed to pH = 8 after the removal of PSS, they immediately swelled back and acquired their initial cubical shape with the corresponding sizes of 8.2 ± 0.6 μm (previously treated with 3 wt % PSS; Figure 9a) and 8.7 ± 0.7 μm (previously treated with 5 wt % PSS; Figure 9b). This is a remarkable observation of the shape restoring in nonspherical ultrathin capsules with sharp vertices and edges. Notably, the capsules' pH-sensitive properties were not affected during the osmotically induced deformations using PSS macromolecules. Thus, the capsule size decreased to 4.6 ± 0.5 and 4.6 ± 0.4 μm for the capsules previously treated with 3 wt % PSS (Figure 9c) and with 5% PSS (Figure 9d), respectively, when the solution

https://doi.org/10.1021/acs.macromol.1c00650
Macromolecules 2021, 54, 9712−9723

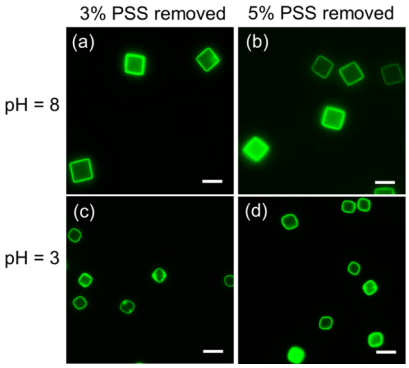

Figure 9. Optical fluorescence images of cubical $(PMAA^*)_{10}$ hydrogel capsules after exposure to 3% (a) and 5% (b) PSS at pH = 3, followed by rinsing off PSS with pH = 3 buffer solution and incubation in pH = 8 buffer solution for 24 h. (c,d) The capsules from (a, b) were transferred to pH = 3 buffer solution. The scale bar is 10 μm in all images.

pH was changed from pH = 8 to pH = 3. This result suggests that the observed slow relaxation of the macroscopic hydrogel structure at low pH is due to the presence of dynamic hydrogen bonds within the network that could interact with PSS at low pH, and the exposure to the basic pH leads to "self-healing" of the cubical shape.

We also tested the initial cubical hydrogen-bonded capsules of $(PMAA^*/PVPON)_{10}$ (Figure 2e) for their deformation behavior at pH = 3. In this case, the network is only physically linked *via* hydrogen bonding without covalent linkages between PMAA layers. The $(PMAA^*/PVPON)_{10}$ capsules obtained after core dissolution in hydrochloric acid followed by rinsing with 1 M HCl were incubated in phosphate buffer solution at pH = 3. Optical fluorescence microscopy revealed that these hydrogen-bonded capsules were of cubical shape and 3.7 ± 0.3 μm in size (a side-to-side distance) (Figure 10a).

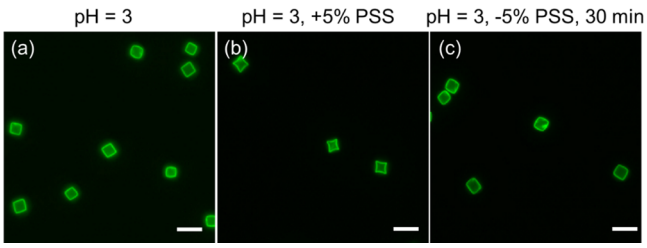

Figure 10. Optical fluorescence images of $(PMAA^*/PVPON)_{10}$ hydrogen-bonded capsules in buffer solution at pH = 3 (a) in the presence of 5 wt % PSS at pH = 3 (b) and 30 min after PSS was rinsed off with buffer solution at pH = 3 (c). The scale bar is 10 μm in all images.

This size was 35% smaller than that for these capsules after being crosslinked and incubated at pH = 3, which agrees with previous reports on hydrogen-bonded spherical and discoidal capsules.[46] These capsules were confirmed by optical fluorescence microscopy to be much more rigid at pH = 3, unlike their hydrogel $(PMAA^*)_{10}$ counterparts when exposed to 5 wt % PSS solution (Figure 10b). They showed low deformations of the faces inward the capsule interior under this osmotic pressure with the s_d = 3 ± 0.3 μm, indicating an enhanced capsule wall stiffness.

Notably, unlike the deformation pattern observed for spherical capsules using the osmotic pressure difference method, where the capsules showed a gradual increase in the number of buckled capsules,[31,53] the cubical hydrogen-bonded capsules showed a uniform response to the applied osmotic pressure. This difference implies that in spherical LbL capsules with physically linked shell networks, the deformations start at the points of nanodefects in the shell, leading to gradual buckling of the capsule population. The deformations are uniform for the whole capsule population in cubical capsules because of the initial higher rigidity points such as vertices and edges.

After rinsing off PSS molecules from the solution, the deformed $(PMAA^*/PVPON)_{10}$ capsules immediately restored their original cubical shape and size (3.7 ± 0.4 μm) upon adding 0.01 M phosphate buffer at pH = 3 (Figure 10c). Again, the stress relaxation behavior was uniform for the whole capsule population. The larger stiffness of the $(PMAA^*/PVPON)_{10}$ capsules is due to a thicker capsule wall because of PVPON layers present in the shell and the abundance of hydrogen-bonded links in the network.

CONCLUSIONS

We synthesized cubical capsules with a nanostructured hydrogel wall obtained through multilayer deposition of hydrogen-bonded PVPON and $PMAA{-}NH_2$ copolymers onto cubical manganese oxide sacrificial microparticles of 5 μm followed by carbodiimide-assisted crosslinking of $PMAA{-}NH_2$ layers, the release of PVPON, and, finally, dissolution of the inorganic cores. We found that the hydrogel capsules obtained from the $PMAA{-}NH_2{-}m$ copolymer with the higher molar ratio of amine groups m = 6.4% compared to that with m = 2.5% could preserve the cubical shape after core dissolution and hydrogel purification from manganese ions using EDTA. These stiffer capsules with an average crosslink density of 16 monomer units between crosslinks also demonstrated a reversible size increase from 4.9 ± 0.6 μm at pH = 3 to 9.0 ± 0.8 μm at pH = 8 with remarkable maintenance of the cubical shape even in the swollen (70%) state of the PMAA multilayer hydrogel shell. We found that at basic pH = 8 and small osmotic pressures (6−20 kN m^{-2}) that were induced by low concentrations (0.1−0.3 wt %) of PSS macromolecules (M_w 70 kDa), the capsules reversibly deformed alongside the cubical faces through inward face buckling. At higher osmotic pressures (>33 kN m^{-2}), the cubical capsules exhibited a complete inward buckling of faces and edges with preserved uncollapsed vertices. These severe deformations were immediately and fully reversible upon stress removal by rinsing off PSS from solution, leading to total regaining of the initial cubical shape and size. The hydrogel shell elasticity estimated using the thin square film bulging approach was found to be ~56 MPa, which is in the range for elastomeric networks.

Unlike immediate regaining of the initial shape at pH = 8 after stress release, the hydrogel capsules at pH = 3 demonstrated a prolonged relaxation from deformations for up to 3 days after PSS removal. This relaxation difference in response to osmotically induced stresses can be attributed to slow stress release hampered by adsorbed PSS. The exposure of the deformed cubical $(PMAA)_{10}$ hydrogel capsules to pH = 8 resulted in instant swelling of the network and restoring the initial cubical shape and size. We also found that cubical capsules of $(PMAA{-}NH_2/PVPON)_{10}$ with only physical links in the hydrogen-bonded network were much stiffer at pH = 3, unlike their hydrogel $(PMAA)_{10}$ counterparts, and demonstrated low deformations of the faces inward the capsule

https://doi.org/10.1021/acs.macromol.1c00650
Macromolecules 2021, 54, 9712−9723

interior under high osmotic pressure. Our experimental data suggest that in contrast to the osmotically induce deformations of spherical capsules that show a gradual increase in the number of buckled capsules, the cubical capsules had a uniform response, implying that the deformations are uniform for the capsule population due to the preset points of rigidity such as vertices and edges. Our study is the first example of nonspherical capsules with nanothin shells (86 nm dry thickness) and sharp vertices and edges that can quickly and fully restore their complex shape after large deformations. Our findings can be essential to the development of adaptable systems for controlled drug delivery.

■ ASSOCIATED CONTENT

Supporting Information

The Supporting Information is available free of charge at https://pubs.acs.org/doi/10.1021/acs.macromol.1c00650.

Chemical structure of Alexa Fluor 488 hydrazide fluorescent dye; representative optical fluorescence microscopy images for analysis of capsule sizes; intensity−distance profiles generated from capsule images using ImageJ software; optical microscopy images of non-labeled capsules buckled in the presence of PSS at pH = 7; and zeta-potential measurements of cubical capsules at pH = 7 and pH = 3 (PDF)

■ AUTHOR INFORMATION

Corresponding Author

Eugenia Kharlampieva − *Department of Chemistry and Center of Nanoscale Materials and Biointegration, The University of Alabama at Birmingham, Birmingham, Alabama 35294, United States;* orcid.org/0000-0003-0227-0920; Email: ekharlam@uab.edu

Authors

Veronika Kozlovskaya − *Department of Chemistry, The University of Alabama at Birmingham, Birmingham, Alabama 35294, United States;* orcid.org/0000-0001-9089-4842

Bing Xue − *Department of Chemistry, The University of Alabama at Birmingham, Birmingham, Alabama 35294, United States*

Maksim Dolmat − *Department of Chemistry, The University of Alabama at Birmingham, Birmingham, Alabama 35294, United States;* orcid.org/0000-0002-4918-7342

Complete contact information is available at: https://pubs.acs.org/10.1021/acs.macromol.1c00650

Author Contributions

V.K. and B.X. equally contributed to this work. The manuscript was written through the contributions of all authors. All authors have given approval to the final version of the manuscript.

Funding

National Science Foundation (NSF) award #1904816.

Notes

The authors declare no competing financial interest.

■ ACKNOWLEDGMENTS

This work was supported by NSF-DMR award #1904816.

■ REFERENCES

(1) Gopal, V.; Kumar, A.; Usha, A.; Karthik, A.; Udupa, N. Effective drug targeting by erythrocytes as carrier systems. *Curr. Trends Biotechnol. Pharm.* **2007**, *1*, 18−33.

(2) Diez-Silva, M.; Dao, M.; Han, J.; Lim, C.-T.; Suresh, S. Shape and biomechanical characteristics of human red blood cells in health and disease. *MRS Bull.* **2010**, *35*, 382−388.

(3) Young, K. D. The selective value of bacterial shape. *Microbiol. Mol. Biol. Rev.* **2006**, *70*, 660−703.

(4) Lautenschläger, F.; Paschke, S.; Schinkinger, S.; Bruel, A.; Beil, M.; Guck, J. The regulatory role of cell mechanics for migration of differentiating myeloid cells. *Proc. Natl. Acad. Sci. U.S.A.* **2009**, *106*, 15696−15701.

(5) Klages, B.; Brandt, U.; Simon, M. I.; Schultz, G.; Offermanns, S. Activation of G12/G13 results in shape change and Rho/Rho-kinase-mediated myosin light chain phosphorylation in mouse platelets. *J. Cell Biol.* **1999**, *144*, 745−754.

(6) Mei, L.; Liu, Y.; Zhang, H.; Zhang, Z.; Gao, H.; He, Q. Antitumor and Antimetastasis activities of Heparin-based Micelle Served As Both Carrier and Drug. *ACS Appl. Mater. Interfaces* **2016**, *8*, 9577−9589.

(7) Perry, J. L.; Herlihy, K. P.; Napier, M. E.; DeSimone, J. M. PRINT: A novel platform toward shape and size specific nanoparticle theranostics. *Acc. Chem. Res.* **2011**, *44*, 990−998.

(8) Blanco, E.; Shen, H.; Ferrari, M. Principles of nanoparticle design for overcoming biological barriers to drug delivery. *Nat. Biotechnol.* **2015**, *33*, 941−951.

(9) Champion, J. A.; Katare, Y. K.; Mitragotri, S. Making polymeric micro- and nanoparticles of complex shapes. *Proc. Natl. Acad. Sci. U.S.A.* **2007**, *104*, 11901−11904.

(10) Tao, L.; Zhao, X. M.; Gao, J. M.; Hu, W. Lithographically defined uniform worm-shaped polymeric nanoparticles. *Nanotechnology* **2010**, *21*, 095301.

(11) Hu, X.; Zhou, J.; Vatankhah-Varnosfaderani, M.; Daniel, W. F. M.; Li, Q.; Zhushma, A. P.; Dobrynin, A. V.; Sheiko, S. S. Programming Temporal Shapeshifting. *Nat. Commun.* **2016**, *7*, 12919.

(12) Zhou, J.; Sheiko, S. S. Reversible shape-shifting in polymeric materials. *J. Polym. Sci., Part B: Polym. Phys.* **2016**, *54*, 1365−1380.

(13) Anselmo, A. C.; Mitragotri, S. Impact of particle elasticity on particle-based drug delivery systems. *Adv. Drug Delivery Rev.* **2017**, *108*, 51−67.

(14) Saxena, S.; Hansen, C. E.; Lyon, L. A. Microgel Mechanics in Biomaterial Design. *Acc. Chem. Res.* **2014**, *47*, 2426−2434.

(15) Zhang, X.; Malhotra, S.; Molina, M.; Haag, R. Micro- and nanogels with labile crosslinks—From synthesis to biomedical applications. *Chem. Soc. Rev.* **2015**, *44*, 1948−1973.

(16) Anselmo, A. C.; Zhang, M.; Kumar, S.; Vogus, D. R.; Menegatti, S.; Helgeson, M. E.; Mitragotri, S. Elasticity of nanoparticles influences their blood circulation, phagocytosis, endocytosis, and targeting. *ACS Nano* **2015**, *9*, 3169−3177.

(17) Merkel, T. J.; Jones, S. W.; Herlihy, K. P.; Kersey, F. R.; Shields, A. R.; Napier, M.; Luft, J. C.; Wu, H.; Zamboni, W. C.; Wang, A. Z.; Bear, J. E.; DeSimone, J. M. Using mechanobiological mimicry of red blood cells to extend circulation times of hydrogel microparticles. *Proc. Natl. Acad. Sci. U.S.A.* **2011**, *108*, 586−591.

(18) Garapaty, A.; Champion, J. A. Tunable Particles Alter Macrophage Uptake Based on Combinatorial Effects of Physical Properties. *Bioeng. Transl. Med.* **2017**, *2*, 92−101.

(19) Brown, T. D.; Habibi, N.; Wu, D.; Lahann, J.; Mitragotri, S. Effect of Nanoparticle Composition, Size, Shape, and Stiffness on Penetration Across the Blood-Brain Barrier. *ACS Biomater. Sci. Eng.* **2020**, *6*, 4916−4928.

(20) Guo, P.; Liu, D.; Subramanyam, K.; Wang, B.; Yang, J.; Huang, J.; Auguste, D. T.; Moses, M. A. Nanoparticle elasticity directs tumor uptake. *Nat. Commun.* **2018**, *9*, 130.

(21) Chen, Y.; Li, X.; Wang, M.; Peng, L.; Yu, Z.; Peng, X.; Song, J.; Qu, J. Virus-Inspired Deformable Mesoporous Nanocomposites for High Efficiency Drug Delivery. *Small* **2020**, *16*, 1906028.

(22) Haghgooie, R.; Toner, M.; Doyle, P. S. Squishy non-spherical hydrogel microparticles. *Macromol. Rapid Commun.* **2010**, *31*, 128−134.
(23) Merkel, T. J.; Chen, K.; Jones, S. W.; Pandya, A. A.; Tian, S.; Napier, M. E.; Zamboni, W. E.; DeSimone, J. M. The effect of particle size on the biodistribution of low-modulus hydrogel PRINT particles. *J. Controlled Release* **2012**, *162*, 37−44.
(24) Kersey, F. R.; Merkel, T. J.; Perry, J. L.; Napier, M. E.; DeSimone, J. M. Effect of aspect ratio and deformability on nanoparticle extravasation through nanopores. *Langmuir* **2012**, *28*, 8773−8781.
(25) Costa, R. R.; Mano, J. F. Polyelectrolyte multilayered assemblies in biomedical technologies. *Chem. Soc. Rev.* **2014**, *43*, 3453−3479.
(26) Cui, J.; Richardson, J. J.; Björnmalm, M.; Faria, M.; Caruso, F. Nanoengineered templated polymer particles: Navigating the biological realm. *Acc. Chem. Res.* **2016**, *49*, 1139−1148.
(27) Yashchenok, A.; Parakhonskiy, B.; Donatan, S.; Kohler, D.; Skirtach, A.; Möhwald, H. Polyelectrolyte multilayer microcapsules templated on spherical, elliptical and square calcium carbonate particles. *J. Mater. Chem. B* **2013**, *1*, 1223−1228.
(28) Kozlovskaya, V.; Kharlampieva, E.; Erel, I.; Sukhishvili, S. A. Multilayer-derived, ultrathin, stimuli-responsive hydrogels. *Soft Matter* **2009**, *5*, 4077−4087.
(29) Kharlampieva, E.; Kozlovskaya, V.; Sukhishvili, S. A. Layer-by-layer hydrogen-bonded polymer films: From fundamentals to applications. *Adv. Mater.* **2009**, *21*, 3053−3065.
(30) Flory, P. J. *Principles of Polymer Chemistry*; Cornell University Press: Ithaca, NY, 1953.
(31) Gao, C.; Donath, E.; Moya, S.; Dudnik, V.; Möhwald, H. Elasticity of hollow polyelectrolyte capsules prepared by the layer-by-layer technique. *Eur. Phys. J. E* **2001**, *5*, 21−27.
(32) Kozlovskaya, V.; Xue, B.; Kharlampieva, E. Shape-adaptable polymeric particles for controlled delivery. *Macromolecules* **2016**, *49*, 8373−8386.
(33) Chong, S.-F.; Lee, J. H.; Zelikin, A. N.; Caruso, F. Tuning the permeability of polymer hydrogel capsules: An investigation of cross-linking density, membrane thickness, and cross-linkers. *Langmuir* **2011**, *27*, 1724−1730.
(34) Kozlovskaya, V.; Kharlampieva, E.; Mansfield, M. L.; Sukhishvili, S. A. Poly(methacrylic acid) hydrogel films and capsules: Response to pH and ionic strength, and encapsulation of macromolecules. *Chem. Mater.* **2006**, *18*, 328−336.
(35) Kozlovskaya, V.; Chen, J.; Zavgorodnya, O.; Hasan, M. B.; Kharlampieva, E. Multilayer hydrogel capsules with interpenetrated network shell for encapsulation of small molecules. *Langmuir* **2018**, *34*, 11832−11842.
(36) She, S.; Li, Q.; Shan, B.; Tong, W.; Gao, C. Fabrication of red-blood-cell-like polyelectrolyte microcapsules and their deformation and recovery behavior through a microcapillary. *Adv. Mater.* **2013**, *25*, 5814−5818.
(37) Alexander, J. F.; Kozlovskaya, V.; Chen, J.; Kuncewicz, T.; Kharlampieva, E.; Godin, B. Cubical shape enhances the interaction of layer-by-layer polymeric particles with breast cancer cells. *Adv. Healthcare Mater.* **2015**, *4*, 2657−2666.
(38) Ejima, H.; Yanai, N.; Best, J. P.; Sindoro, M.; Granick, S.; Caruso, F. Near-incompressible faceted polymer microcapsules from metal-organic framework templates. *Adv. Mater.* **2013**, *25*, 5767−5771.
(39) Shchepelina, O.; Kozlovskaya, V.; Kharlampieva, E.; Mao, W.; Alexeev, A.; Tsukruk, V. V. Anisotropic Micro- and Nano-Capsules. *Macromol. Rapid Commun.* **2010**, *31*, 2041−2046.
(40) Chen, X.; Cui, J.; Sun, H.; Müllner, M.; Yan, Y.; Noi, K. F.; Ping, Y.; Caruso, F. Analysing intracellular deformation of polymer capsules using structured illumination microscopy. *Nanoscale* **2016**, *8*, 11924−11931.
(41) Liang, X.; Kozlovskaya, V.; Chen, Y.; Zavgorodnya, O.; Kharlampieva, E. Thermosensitive Multilayer Hydrogels of Poly(N-vinylcaprolactam) as Nanothin Films and Shaped Capsules. *Chem. Mater.* **2012**, *24*, 3707−3719.
(42) Kozlovskaya, V.; Wang, Y.; Higgins, W.; Chen, J.; Chen, Y.; Kharlampieva, E. pH-Triggered Shape Response of Cubical Ultrathin Hydrogel Capsules. *Soft Matter* **2012**, *8*, 9828−9839.
(43) Kozlovskaya, V.; Stockmal, K. A.; Higgins, W.; Ankner, J. F.; Morgan, S. E.; Kharlampieva, E. Architecture of Hydrated Multilayer Poly(methacrylic acid) Hydrogels: Effect of Solution pH. *ACS Appl. Polym. Mater.* **2020**, *2*, 2260−2273.
(44) Kozlovskaya, V.; Chen, J.; Tedjo, C.; Liang, X.; Campos-Gomez, J.; Oh, J.; Saeed, M.; Lungu, C. T.; Kharlampieva, E. pH-Responsive Hydrogel Cubes for Release of Doxorubicin in Cancer Cells. *J. Mater. Chem. B* **2014**, *2*, 2494−2507.
(45) Kozlovskaya, V.; Higgins, W.; Chen, J.; Kharlampieva, E. Shape switching of hollow layer-by-layer hydrogel microcontainers. *Chem. Commun.* **2011**, *47*, 8352−8354.
(46) Kozlovskaya, V.; Alexander, J. F.; Wang, Y.; Kuncewicz, T.; Liu, X.; Godin, B.; Kharlampieva, E. Internalization of Red Blood Cell-mimicking Hydrogel Capsules with pH-triggered Shape Responses. *ACS Nano* **2014**, *8*, 5725−5737.
(47) Kozlovskaya, V.; Higgins, W.; Chen, J.; Kharlampieva, E. Shape switching of hollow layer-by-layer hydrogel microcontainers. *Chem. Commun.* **2011**, *47*, 8352−8354.
(48) Best, J. P.; Neubauer, M. P.; Javed, S.; Dam, H. H.; Fery, A.; Caruso, F. Mechanics of pH-responsive hydrogel capsules. *Langmuir* **2013**, *29*, 9814−9823.
(49) Best, J. P.; Javed, S.; Richardson, J. J.; Cho, K. L.; Kamphuis, M. M. J.; Caruso, F. Stiffness-mediated adhesion of cervical cancer cells to soft hydrogel films. *Soft Matter* **2013**, *9*, 4580−4584.
(50) Xue, B.; Kozlovskaya, V.; Liu, F.; Chen, J.; Williams, J. F.; Campos-Gomez, J.; Saeed, M.; Kharlampieva, E. Intracellular degradable hydrogel cubes and spheres for anticancer drug delivery. *ACS Appl. Mater. Interfaces* **2015**, *7*, 13633−13644.
(51) Ghaemi, A.; Philipp, A.; Bauer, A.; Last, K.; Fery, A.; Gekle, S. Mechanical behavior of microcapsules and their rupture under compression. *Chem. Eng. Sci.* **2016**, *142*, 236−243.
(52) Knoche, S.; Kierfeld, J. Osmotic buckling of spherical capsules. *Soft Matter* **2014**, *10*, 8358−8369.
(53) Gao, C.; Leporatti, S.; Moya, S.; Donath, E.; Möhwald, H. Stability and mechanical properties of polyelectrolyte capsules obtained by stepwise assembly of poly(styrenesulfonate sodium salt) and poly(diallyldimethyl ammonium) chloride onto melamine resin particles. *Langmuir* **2001**, *17*, 3491−3495.
(54) Gupta, N.; Kozlovskaya, V.; Dolmat, M.; Kharlampieva, E. Shape Recovery of Spherical Hydrogen-Bonded Multilayer Capsules after Osmotically Induced Deformation. *Langmuir* **2019**, *35*, 10910−10919.
(55) Monnier, S.; Delarue, M.; Brunel, B.; Dolega, M. E.; Delon, A.; Cappello, G. Effect of an osmotic stress on multicellular aggregates. *Methods* **2016**, *94*, 114−119.
(56) Chen, J.; Kozlovskaya, V.; Goins, A.; Campos-Gomez, J.; Saeed, M.; Kharlampieva, E. Biocompatible shaped particles from dried multilayer polymer capsules. *Biomacromolecules* **2013**, *14*, 3830−3841.
(57) Poilane, C.; Delobelle, P.; Bornier, L.; Mounaix, P.; Melique, X.; Lippens, D. Determination of the mechanical properties of thin polyimide films deposited on a GaAs substrate by bulging and nanoindentation tests. *Mater. Sci. Eng., A* **1999**, *262*, 101−106.
(58) Chen, K.-S.; Ou, K.-S. MEMS Residual Stress Characterization. In *Handbook of Silicon Based MEMS Materials and Technologies*, 2nd ed.; Tilli, M., Motooka, T., Airaksinen, V.-M., Franssila, S., Paulasto-Kröckel, M., Lindroos, V., Eds.; Micro and Nano Technologies; William Andrew Publishing, 2015; pp 398−412.
(59) Liu, F.; Kozlovskaya, V.; Zavgorodnya, O.; Martinez-Lopez, C.; Catledge, S.; Kharlampieva, E. Encapsulation of anticancer drug with hydrogen-bonded multilayers of tannic acid. *Soft Matter* **2014**, *10*, 9237−9247.
(60) Geissler, E.; Hecht, A. M. The Poisson Ratio in Polymer Gels. *Macromolecules* **1980**, *13*, 1276−1280.

https://doi.org/10.1021/acs.macromol.1c00650
Macromolecules 2021, 54, 9712−9723

(61) Lulevich, V. V.; Andrienko, D.; Vinogradova, O. I. Elasticity of Polyelectrolyte Multilayer Microcapsules. *J. Chem. Phys.* **2004**, *120*, 3822−3826.
(62) Elsner, N.; Kozlovskaya, V.; Sukhishvili, S. A.; Fery, A. pH-Triggered Sofening of crosslinked hydrogen-bonded capsules. *Soft Mater.* **2006**, *2*, 966−972.
(63) Drachuk, I.; Shchepelina, O.; Lisunova, M.; Harbaugh, S.; Kelley-Loughnane, N.; Stone, M.; Tsukruk, V. V. pH-Responsive Layer-by-Layer Nanoshells for Direct Regulation of Cell Activity. *ACS Nano* **2012**, *6*, 4266−4278.
(64) She, S.; Xu, C.; Yin, X.; Tong, W.; Gao, C. Shape deformation and recovery of multilayer microcapsules after being squeezed through a microchannel. *Langmuir* **2012**, *28*, 5010−5016.
(65) She, S.; Li, Q.; Shan, B.; Tong, W.; Gao, C. Fabrication of red blood-cell-like polyelectrolyte microcapsules and their deformation and recovery behavior through a microcapillary. *Adv. Mater.* **2013**, *25*, 5814−5818.
(66) Yang, X.; Cranston, E. D. Chemically cross-linked cellulose nanocrystal aerogels with shape recovery and superabsorbent properties. *Chem. Mater.* **2014**, *26*, 6016−6025.
(67) Zhang, Y.; Liao, J.; Wang, T.; Sun, W.; Tong, Z. Polyampholyte hydrogels with pH modulated shape memory and spontaneous actuation. *Adv. Funct. Mater.* **2018**, *28*, 1707245.
(68) Jeon, I.; Cui, J.; Illeperuma, W. R.; Aizenberg, J.; Vlassak, J. J. Extremely stretchable and fast self-healing hydrogels. *Adv. Mater.* **2016**, *28*, 4678−4683.
(69) Wang, X.; Ye, X.; Zhang, G. Investigation of pH-induced conformational change and hydration of poly(methacrylic acid) by analytical ultracentrifugation. *Soft Matter* **2015**, *11*, 5381−5388.
(70) Todica, M.; Pop, C. V.; Udrescu, L.; Traian, S. Spectroscopy of a Gamma Irradiated Poly(Acrylic Acid)-Clotrimazole System. *Chin. Phys. Lett.* **2011**, *28*, 128201.
(71) Kozlovskaya, V.; Baggett, J.; Godin, B.; Liu, X.; Kharlampieva, E. Hydrogen-Bonded Multilayers of Silk Fibroin: From Coatings to Cell-Mimicking Shaped Microcontainers. *ACS Macro Lett.* **2012**, *1*, 384−387.

https://doi.org/10.1021/acs.macromol.1c00650
Macromolecules 2021, 54, 9712−9723